• Investigation •

Orbital anatomical variations between the Southern China and the Kashi populations based on 3D-CT analysis

Meng Wang[1], Yao Yang[1], Shu-Juan Cao[2], Jun-Jie Tang[1], Jin-Miao Li[1], Yue-Kun Bao[1], Zhi-Hui Zhang[1], Yang Gao[1], Yao-Ming Liu[1], Mayila•Kuerban[2], Tuxungu•Abulizi[2], Shi-Cai Su[1], Wei-Feng Huang[1], Ai-Xin Jiang[2], Rong Lu[1]

[1]State Key Laboratory of Ophthalmology, Zhongshan Ophthalmic Center, Sun Yat-sen University, Guangdong Provincial Key Laboratory of Ophthalmology and Visual Science, Guangdong Provincial Clinical Research Center for Ocular Diseases, Guangzhou 510060, Guangdong Province, China

[2]Ophthalmologic Center, The Affiliated Kashi Hospital of Sun Yat-sen University, The First People's Hospital of Kashi, Kashi 844000, Xinjiang Uygur Autonomous Region, China

Co-first Authors: Meng Wang and Yao Yang

Correspondence to: Rong Lu. State Key Laboratory of Ophthalmology, Zhongshan Ophthalmic Center, Sun Yat-sen University, Guangdong Provincial Key Laboratory of Ophthalmology and Visual Science, Guangdong Provincial Clinical Research Center for Ocular Diseases, Guangzhou 510060, Guangdong Province, China. lurong@gzzoc.com; rongluzz@yahoo.com; Ai-Xin Jiang. Ophthalmologic Center, The Affiliated Kashi Hospital of Sun Yat-sen University, The First People's Hospital of Kashi, Kashi 844000, Xinjiang Uygur Autonomous Region, China. jiangaixinks@163.com

Received: 2025-03-06 Accepted: 2026-01-05

Abstract

• **AIM:** To characterize regional variations in orbital morphology between populations from Southern China and Kashi through three-dimensional computed tomography (3D-CT) measurements, providing anatomical references for clinical practice.

• **METHODS:** In this observational cross-sectional study, patients from Zhongshan Ophthalmic Center (Southern China group) and the First People's Hospital of Kashi (Kashi group) were analyzed using Mimics Research software. And 24 orbital parameters were measured, including orbital volume, retroorbital fat, extraocular muscle volume, and various orbital dimensions.

• **RESULTS:** A total of 160 eyes from 80 participants were included, with each center enrolling 40 participants, comprising 20 males and 20 females. The mean age was 42.75±10.83y (range, 25–58) in the Southern China male group, 48.35±13.04y (range, 21–76) in the Southern China female group, 42.40±17.05y (range, 21–76) in the Kashi male group, and 43.05±13.52y (range, 19–74) in the Kashi female group. No significant differences were observed in orbital volume or medial orbital depth (P>0.05). The Southern China group had greater orbital height (35.98±1.66 *vs* 34.83±1.88 mm; P=0.005), higher orbital index (95.55±6.59 *vs* 91.91±4.72; P=0.006), and larger exophthalmos (16.60±2.15 *vs* 15.49±1.81 mm; P=0.014), while the Kashi group had smaller sphenoid trigone length (11.25±3.14 *vs* 12.64±3.19 mm; P=0.033) and width [7.43 (3.02) mm *vs* 8.83 (3.26) mm; P=0.016]. These differences were mainly observed in males. All 3D-CT measurements showed excellent interobserver reliability (ICC=0.95–0.99).

• **CONCLUSION:** This study reveals distinct regional variations in orbital anatomy between the Southern China and Kashi populations. Participants from Southern China exhibit greater orbital height, orbital index, and exophthalmos, whereas those from Kashi show smaller sphenoid trigone dimensions. These findings provide valuable anatomical references for orbital decompression, fracture reconstruction, and radiological diagnosis.

• **KEYWORDS:** orbital anatomy; computed tomography; geometric measurement; region variations

DOI:10.18240/ijo.2026.07.19

Citation: Wang M, Yang Y, Cao SJ, Tang JJ, Li JM, Bao YK, Zhang ZH, Gao Y, Liu YM, Kuerban M, Abulizi T, Su SC, Huang WF, Jiang AX, Lu R. Orbital anatomical variations between the Southern China and the Kashi populations based on 3D-CT analysis. *Int J Ophthalmol* 2026;19(7):1374-1382

INTRODUCTION

The orbit, situated between cranial and facial bones, provides structural support for the ocular accessory apparatus and serves as a conduit for nerves and blood vessels, housing a significant amount of neurovascular tissue[1-2]. Diseases and surgical injuries affecting the orbit can greatly impair its function[3-4].

Orbital morphology varies significantly with age, gender, and geographic or ethnic background, and plays a central role in the diagnosis and management of ophthalmic diseases[5-8]. For instance, patients with thyroid-related eye diseases often exhibit smaller orbital apex volumes and larger extraocular muscle diameters[9-11]. Furthermore, anatomical variations in the medial orbital wall can impact the safety and efficacy of orbital decompression surgery for thyroid-related eye diseases, while the width of the trigone predicts the reduction of proptosis after deep lateral wall decompression[6,10]. Additionally, differences in orbital anatomy affect the reconstruction of orbital floor fractures[12-13]. Therefore, understanding these anatomical differences is crucial for improving the precision of diagnosis and treatment, as well as achieving accurate surgical outcomes. China encompasses a broad geographic and demographic landscape, with substantial variation across regions[14]. Kashi, situated on China's western border in Xinjiang, is inhabited by multiple ethnic groups such as Uighur, Han, Tajik, Hui, Kyrgyz, Uzbek, and Kazakh[14]. In stark contrast, southern China is predominantly populated by the Han ethnic group, accounting for over 90% of its residents[14]. Although numerous studies have documented anatomical differences in the orbits among various racial groups[15-18], there remains a dearth of research on orbital structural disparities among regions within China. This research gap significantly hampers the accuracy of diagnosing and treating orbital diseases in diverse regions. Therefore, this study aims to comprehensively evaluate orbital structural differences between populations in Kashi and Southern China using three-dimensional computed tomography (3D-CT) measurements, thereby providing region-specific anatomical insights that can refine diagnostic accuracy, optimize surgical strategies, and enhance personalized risk stratification in orbital procedures.

PARTICIPANTS AND METHODS

Ethical Approval The study adhered to the ethical principles of the Declaration of Helsinki and was approved by the Medical Ethics Committees of Zhongshan Ophthalmic Center (No. 2024KYPJ057) and the First People's Hospital of Kashi (No. 2023KSYD87). The requirement for informed consent was waived by the ethics committees due to the retrospective nature of the study and the use of anonymized imaging data.

Participants This observational, retrospective study included patients identified from the imaging databases of Zhongshan Ophthalmic Center, Sun Yat-sen University, and the First People's Hospital of Kashi between January 2019 and December 2023. Patients included in this study were identified from the imaging databases of two hospitals. All enrolled patients had undergone orbital CT scans for clinical indications such as craniofacial trauma, paranasal sinus disease, lacrimal duct disorders, or other relevant conditions, with the imaging field covering the orbital region. After a comprehensive clinical and radiological review by two independent researchers, patients were included if they met the following criteria: 1) no radiological or clinical evidence of orbital disease; 2) no history of orbital surgery. Eligible patients were randomized using stratified sampling by region and sex. The patient selection and allocation process is illustrated in Figure 1. A computer-generated randomization table, prepared by an independent biostatistician, ensured unbiased group allocation. Comparison of age among the four groups using one-way analysis of variance (ANOVA) revealed no significant differences (P>0.05), confirming the validity of the randomization process.

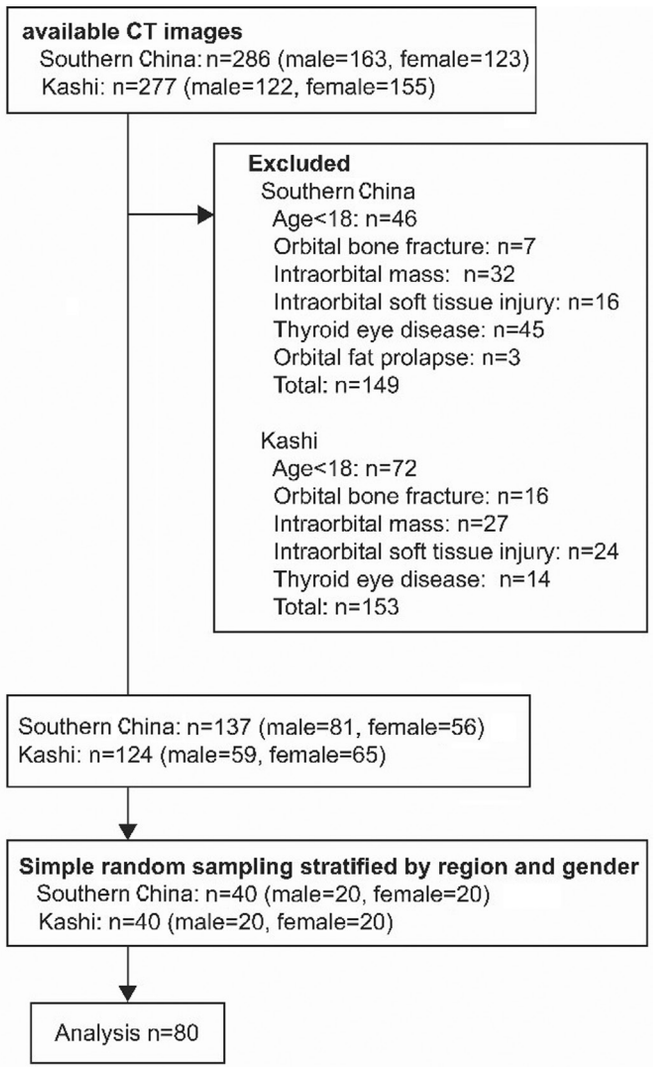

Figure 1 Flow diagram of participant selection CT: Computed tomography.

Orbital Computed Tomography Scan CT data were obtained using CT scanners (SOMATOM Definition for the Kashi cohort and SOMATOM Force for the Southern China cohort; Siemens Healthineers, Germany). Uniform parameters were applied across centers: 120 kV, 80–100 mAs, 1 mm slice thickness, and 1 mm interval. Scans were obtained in the supine position with patients fixating on a designated point to

minimize ocular motion. The scanning range extended from the infraorbital margin to the superior orbital rim.

Measurements CT data were processed and reconstructed using Mimics Research software (version 19.0; Leuven, Belgium). All measurements were performed by a single experienced observer, with a second observer performing partial measurements to assess interobserver reliability. Orbital structures were segmented by adjusting the image window ranges according to tissue density: −226 to 2240 Hounsfield units (HU) for bone, −200 to −30 HU for adipose tissue, −30 to +100 HU for extraocular muscles, and −200 to +100 HU for the orbital volume (OV), following the approach of Bao *et al*[11] (Figure 2A). Key anatomical landmarks on the 3D orbital bone models (Figure 2B) were identified according to the reference scheme of Hierl *et al*[5]. Orbital measurements were categorized into two major domains according to anatomical relevance: 1) orbital morphology parameters; 2) interorbital and lateral orbital parameters.

The orbital morphology parameters, including the primary endpoints of OV, exophthalmos, medial orbital depth, orbital width, orbital height, and orbital index (OI), were measured as follows: 1) OV (cm³): The total 3D volume enclosed by the orbital walls; 2) Exophthalmos (mm): The perpendicular distance from the apex of the cornea to the line connecting the midpoints of the lateral orbital rims; 3) Medial orbital depth (mm): The distance from the dacryon (the junction of the maxilla, lacrimal bone, and frontal bone) to the central point of optic canal; 4) Orbital width (mm): The distance from the midpoint of the lateral orbital rim to the dacryon; 5) Orbital height (mm): The distance from the midpoint of the superior orbital rim to the midpoint of the inferior orbital rim; 6) OI: Calculated as orbital height/orbital width×100.

Additional secondary endpoints included: 1) Extraocular muscle volume (cm³): The combined volume of the four rectus muscles segmented according to tissue density; 2) Retroorbital fat volume (cm³): The volume of adipose tissue within the orbit, calculated as the total OV minus the volumes of the eyeball and extraocular muscles; 3) Orbital depth (mm): The distance from the midpoint of the line connecting the lateral orbital rim and dacryon to the central point of the optic canal; 4) Lateral orbital depth (mm): The distance from the midpoint of the lateral orbital rim to the central point of optic canal; 5) Superior orbital depth (mm): The distance from the superior orbital rim to the optic canal; 6) Inferior orbital depth (mm): The distance from the inferior orbital rim to the optic canal; 7) Intraorbital optic nerve length (mm): The distance between the optic nerve–eyeball junction and the central point of the optic canal; 8) Horizontal orbital angle (°): The angle formed at the optic canal apex, with arms extending to the lateral orbital rim midpoint and the dacryon (Figure 2C); 9) Vertical orbital angle (°): The angle formed at the optic canal apex, with arms extending to the midpoints of the superior and inferior orbital rims (Figure 2C).

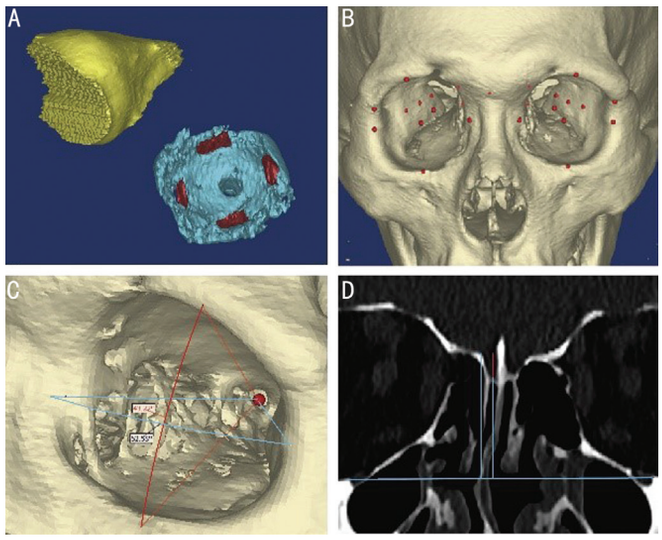

Figure 2 Illustration of orbital measurements in the 3D models A: 3D reconstruction of orbital volume (yellow), retroorbital fat volume (blue), and extraocular muscle volume (red); B: Anatomical points: red dots represent the marked anatomical landmarks; C: Horizontal orbital angle (blue) and vertical orbital angle (red); D: OF depth, represented by the red line, is defined as the difference between the vertical distances from the ethmoid roof and the cribriform plate to the line connecting the bilateral infraorbital canals (blue). 3D: Three-dimension; OF: Olfactory fossa.

The interorbital and lateral orbital parameters, including the primary endpoints of olfactory fossa (OF) depth, sphenoid trigone length, and sphenoid trigone width, were measured as follows: 1) OF depth (mm): measured on the slice showing the deepest cribriform plate, calculated as the vertical distance difference between the ethmoid roof and the cribriform plate relative to the horizontal line connecting the bilateral infraorbital canals, with KEROS classification defined as Type I (<4 mm), Type II (4–7 mm), and Type III (>7 mm; Figure 2D)[19]; 2) Sphenoid trigone length (mm): the length of the sphenoid trigone in the horizontal orbital angle plane; 3) Sphenoid trigone width (mm): the width of the sphenoid trigone in the horizontal orbital angle plane.

Additional secondary end points included: 1) Inter-optic canal distance (mm): the distance between the centers of the two optic canals; 2) Anterior interorbital distance (mm): the distance between the bilateral dacryons; 3) Middle interorbital distance (mm): the distance between the midpoints of the bilateral medial orbital walls; 4) Lateral orbital rim midpoint distance (mm): the distance between the midpoints of the bilateral lateral orbital rims; 5) Lateral orbit-posterior sphenoid distance (mm): the distance from the midpoint of the lateral orbital rim to the posterior edge of the sphenoidal trigone in

Table 1 Comparison of orbital parameters between the Southern China and the Kashi populations mean±SD

Parameters	Southern China (*n*=40)	Kashi (*n*=40)	*Z*/*t*	*P*[a]
OV (cm^3)	24.99±2.32	25.16±2.38	-0.319	0.750
Medial orbital depth (mm)	40.70±2.46	41.62±2.57	-1.632	0.107
Orbital width (mm)	37.75±1.89	37.89±1.85	-0.317	0.752
Orbital height (mm)	35.98±1.66	34.83±1.88	2.887	0.005
OI	95.55±6.59	91.91±4.72	2.840	0.006
Exophthalmos (mm)	16.60±2.15	15.49±1.81	2.512	0.014

[a]Independent samples *t*-test. OV: Orbital volume; OI: Orbital index; SD: Standard deviation. *P*<0.05 was considered statistically significant.

the horizontal orbital angle plane; 6) Lateral orbit–anterior sphenoid distance (mm): the distance from the midpoint of the lateral orbital rim to the anterior edge of the sphenoidal trigone in the horizontal orbital angle plane.

Reliability Assessment Interobserver consistency was quantified using the intraclass correlation coefficient (ICC), with values above 0.90 interpreted as indicating excellent reliability. All measurements of the five representative parameters (OV, exophthalmos, orbital depth, orbital height, and horizontal orbital angle) were used for interobserver reliability analysis. Systematic differences between observers were further assessed by evaluating fixed bias, using a one-sample *t*-test to compare the mean difference against zero, and proportional bias, using linear regression analysis of the differences versus the means of the two measurements. A *P* value<0.05 was considered statistically significant.

Statistical Analysis Statistical analysis was conducted using IBM SPSS Statistics (version 25.0, IBM Corp., Armonk, NY, USA). The average values of both eyes of each participant were used for the analysis. Normality was tested using the Shapiro-Wilk test. Data were presented according to their distribution: mean±standard deviation (SD) for normally distributed variables, and median (interquartile range) for non-normally distributed variables. Independent samples *t*-tests were used for normally distributed variables, and Mann-Whitney *U* tests for non-normally distributed variables, with statistical significance set at *P*<0.05. For secondary outcomes, multiple comparisons were adjusted using the Benjamini-Hochberg method to control the false discovery rate (FDR), with an FDR-adjusted *P* value<0.05 considered statistically significant. Categorical variables (Keros types) were compared using Fisher's exact test with Monte Carlo simulation (*P*<0.05 considered significant).

RESULTS

Demographic Distribution A total of 160 eyes from 80 participants were included, with each center enrolling 40 participants, comprising 20 males and 20 females. The mean age was 42.75±10.83y (range, 25–58) in the Southern China male group, 48.35±13.04y (range, 21–76) in the Southern China female group, 42.40±17.05y (range, 21–76) in the Kashi male group, and 43.05±13.52y (range, 19–74) in the Kashi female group. One-way ANOVA showed no significant difference in age among the four groups (*P*=0.892), confirming comparability between groups.

Differences in Orbital Parameters Primary orbital parameters were compared between the Southern China and Kashi groups. No significant differences were observed in OV or medial orbital depth (*P*>0.05; Table 1; Figure 3B). However, the Southern China group exhibited significantly greater orbital height (35.98±1.66 *vs* 34.83±1.88 mm, *P*=0.005), while orbital width was comparable between groups (*P*=0.752; Figure 3A). Consequently, the OI was significantly higher in Southern participants (95.55±6.59 *vs* 91.91±4.72, *P*=0.006). Exophthalmos was also significantly greater in the Southern group compared to Kashi participants (16.60±2.15 *vs* 15.49±1.81 mm, *P*=0.014; Figure 3C, 3D). Other secondary parameters showed no significant differences after FDR correction (FDR>0.05; Table 2).

Differences in Interorbital and Lateral Orbital Anatomy Parameters When comparing the interorbital anatomical structures between the two groups, no significant difference was observed in OF depth (*P*>0.05, Table 3). Although Keros type III was present in 4 cases (10.00%) in the Southern China group and 1 case (2.50%) in the Kashi group, the overall distribution of Keros types did not differ significantly (*P*>0.05, Table 3). Analysis of the lateral orbital wall showed that the Kashi group (Figure 4A) had a significantly smaller sphenoid trigone length (11.25±3.14 *vs* 12.64±3.19 mm, *P*=0.033) and width [7.43 (3.02) *vs* 8.83 (3.26) mm, *P*=0.016] compared to the Southern China group (Figure 4B). Regarding the secondary endpoints, although slight differences were observed in the lateral orbit-posterior sphenoid distances, they were not significant after FDR correction, and no significant differences were found for the remaining secondary endpoints (FDR>0.05, Table 2).

Sex-Stratified Analysis of Primary Endpoints Considering the potential influence of sex on orbital anatomy, we performed a sex-stratified analysis of the primary endpoints (Table 4). Male participants from the Kashi region exhibited significantly lower exophthalmos, orbital height, and OI compared to their

Table 2 Comparison of secondary endpoints between Southern China and Kashi populations mean±SD or median (interquartile range)

Parameters	The Southern (*n*=40)	The Kashi (*n*=40)	*Z*/*t*	*P*	FDR
Retroorbital fat volume (cm^3)	10.84±2.19	10.48±2.08	0.760	0.450[a]	0.881
Extraocular muscle volume (cm^3)	28.52±5.70	28.72±4.85	-0.228	0.820[a]	0.881
Orbital depth (mm)	39.48±2.00	39.99±2.16	-1.084	0.282[a]	0.881
Lateral orbital depth (mm)	46.85±2.10	46.25±1.87	1.336	0.186[a]	0.698
Superior orbital depth (mm)	49.39±2.22	49.69±2.36	-0.586	0.560[a]	0.881
Inferior orbital depth (mm)	47.54±2.17	48.07±2.58	-0.991	0.325[a]	0.881
Intra-orbital optic nerve length (mm)	27.18±3.10	26.93±2.28	0.406	0.686[a]	0.881
Horizontal orbital angle (°)	50.63±2.56	50.57±2.97	0.097	0.923[a]	0.923
Vertical orbital angle (°)	43.09 (3.43)	42.70 (8.58)	-0.327	0.774[b]	0.881
Inter-optic Canal distance (mm)	29.87±3.43	30.02±2.60	-0.225	0.822[a]	0.881
Middle interorbital distance (mm)	27.26±3.51	27.67±3.27	-0.543	0.589[a]	0.881
Anterior interorbital distance (mm)	23.89 (2.72)	24.84 (3.33)	-1.848	0.065[b]	0.488
Lateral orbital rim midpoint distance (mm)	97.14±4.08	97.35±4.00	-0.230	0.819[a]	0.881
Lateral orbit-anterior sphenoid distance (mm)	17.47 (2.59)	17.61 (2.25)	-0.231	0.817[b]	0.881
Lateral orbit-posterior sphenoid distance (mm)	30.20±3.92	28.51±3.38	2.057	0.043[a]	0.488

[a]Independent samples *t*-test; [b]The Mann-Whitney *U* test. FDR: False discovery rate; SD: Standard deviation. FDR<0.05 was considered statistically significant.

Table 3 Comparison of interorbital and lateral orbital anatomy between the Southern China and the Kashi populations

mean±SD or median (interquartile range)

Parameters	Southern China (*n*=40)	Kashi (*n*=40)	*Z*/*t*	RR (95%CI)	OR (95%CI)	*P*
Sphenoid trigone length (mm)	12.64±3.19	11.25±3.14	2.174			0.033[a]
Sphenoid trigone width (mm)	8.83 (3.26)	7.43 (3.02)	2.400			0.016[b]
OF depth (mm)	5.22 (2.16)	5.01 (1.74)	0.433			0.665[b]
Keros type I, *n* (%)	7 (17.50)	5 (12.50)		1.06 (0.88-1.28)	1.48 (0.43-5.14)	0.290[c]
Keros type II, *n* (%)	29 (72.50)	34 (85.00)		0.55 (0.22-1.33)	0.47 (0.15-1.41)	0.290[c]
Keros type III, *n* (%)	4 (10.00)	1 (2.50)		1.08 (0.97-1.21)	4.33 (0.46-40.61)	0.290[c]

[a]Independent samples *t*-test; [b]The Mann-Whitney *U* test; [c]Fisher's exact test. OF: Olfactory fossa; RR: Relative risk; CI: Confidence interval; OR: Odds ratio; SD: Standard deviation. *P*<0.05 was considered statistically significant.

Table 4 Sex-stratified characteristics of differentiated parameters mean±SD or median (interquartile range)

Parameters	Male			Female		
	Southern China (*n*=20)	Kashi (*n*=20)	*P*	Southern China (*n*=20)	Kashi (*n*=20)	*P*
OV (cm^3)	26.00±2.21	26.39±1.87	0.536[a]	24.00±2.00	23.93±2.28	0.929[a]
Exophthalmos (mm)	17.15 (2.82)	15.97 (1.60)	0.005[b]	15.54±1.73	15.32±1.95	0.714[a]
Orbital width (mm)	38.66±1.41	38.59±1.74	0.884[a]	36.84±1.90	37.18±1.73	0.558[a]
Orbital height (mm)	36.19±1.53	34.82±1.53	0.007[a]	35.76±1.79	34.84±2.22	0.158[a]
OI	93.71±4.68	89.90±2.70	0.003[a]	97.40±7.76	93.91±5.48	0.109[a]
Sphenoid trigone length (mm)	12.56±2.69	11.31±2.68	0.151[a]	12.73±3.21	11.20±2.97	0.124[a]
Sphenoid trigone width (mm)	9.30±2.19	8.06±2.84	0.130[a]	8.45 (3.47)	7.74 (3.47)	0.192[b]
OF depth (mm)	5.76±2.09	5.29±1.21	0.390[a]	4.96±1.20	4.93±1.08	0.993[a]

[a]Independent samples *t*-test; [b]The Mann-Whitney *U* test. OV: Orbital volume; OI: Orbital index; OF: Olfactory fossa. *P*<0.05 was considered statistically significant.

Southern China counterparts ($P<0.05$). In contrast, female participants showed no significant regional differences. Notably, after stratification by sex, sphenoid trigone length and width no longer differed between regions, whereas these measures had been significantly larger in Southern China participants before stratification.

Reliability Assessment of 3D-CT Measurements To assess the interobserver reliability of 3D-CT measurements, five representative parameters were analyzed, including OV, exophthalmos, orbital depth, orbital height, and horizontal orbital angle. All parameters showed excellent reliability, with intraclass correlation coefficients (ICCs) ranging from 0.950

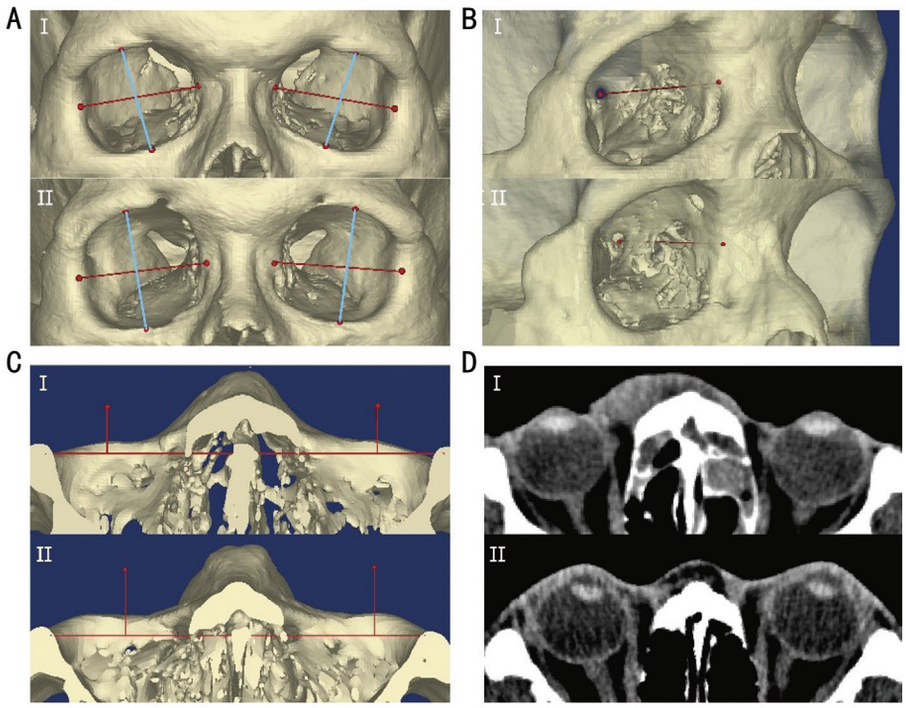

Figure 3 Comparison of orbital anatomy between the Southern China and Kashi populations A: The orbital height (blue) and the orbital width (red) of a Kashi participant (I) and a Southern China participant (II); B: The medial orbital depth (red) of a Kashi participant (I) and a Southern China participant (II); C: Exophthalmos measurement and the reference line connecting the midpoints of the lateral orbital rims (red) in a Kashi participant (I) and a Southern China participant (II); D: Corresponding CT images for exophthalmos measurement in the Kashi participant (I) and the Southern China participant (II). CT: Computed tomography.

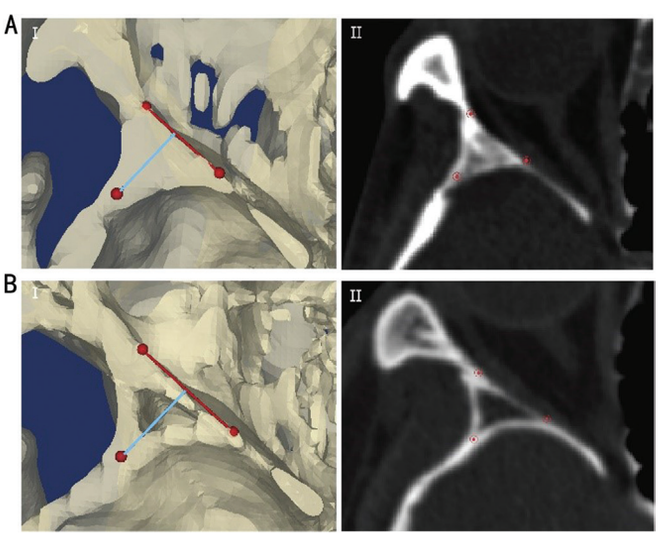

Figure 4 Comparison of sphenoid trigone anatomy between the Southern China and Kashi populations A: Sphenoid trigone length (red) and width (blue) in a representative Kashi participant (I) and corresponding CT image (II); B: Sphenoid trigone length (red) and width (blue) in a representative Southern China participant (I) and corresponding CT image (II). CT: Computed tomography.

for orbital height to 0.988 for OV and horizontal orbital angle. The 95% confidence intervals for fixed bias included zero for all parameters, indicating no fixed bias, and all proportional bias tests yielded *P* values above 0.05, confirming the absence of proportional bias (Table 5).

DISCUSSION

This study revealed significant regional differences in orbital anatomy between populations from Southern China and Kashi. Compared with the Southern China cohort, the Kashi cohort exhibited smaller orbital height, OI, and exophthalmos, as well as shorter and narrower sphenoid trigone dimensions. These findings provide essential anatomical insights for region-specific clinical assessment and support individualized surgical planning tailored to local anatomical characteristics.

To further refine these observations, we performed a sex-stratified analysis of the primary endpoints. Among males, the Kashi group showed significantly lower exophthalmos, orbital height, and OI than their Southern China counterparts, whereas no regional differences were observed in females. Notably, the previously significant differences in sphenoid trigone length and width disappeared after stratification, suggesting that these regional variations were largely driven by male participants. Nevertheless, as sex stratification substantially reduced subgroup sample sizes and statistical power, the absence of significant differences in females or in sphenoid trigone morphology should be interpreted with caution. These findings underscore the importance of incorporating sex-specific reference values when interpreting orbital morphometry and planning surgical interventions.

Table 5 Relative and absolute reliability of 3D-CT analysis

Parameters	ICC (95%CI)	Fixed bias		Proportional bias	
		95%CI	Existence	*P*	Existence
OV (*n*=80)	0.988 (0.981 to 0.992)	-0.06 to 0.10	No	0.367	No
Exophthalmos (*n*=80)	0.971 (0.956 to 0.982)	-0.18 to 0.04	No	0.350	No
Orbital depth (*n*=80)	0.951 (0.924 to 0.968)	-0.03 to 0.26	No	0.316	No
Orbital height (*n*=80)	0.950 (0.923 to 0.968)	-0.21 to 0.06	No	0.367	No
Horizontal orbital angle (*n*=80)	0.948 (0.920 to 0.966)	-0.29 to 0.11	No	0.904	No

Interobserver consistency was quantified using ICC, with values greater than 0.90 indicating excellent reliability. Fixed bias was evaluated using a one-sample *t*-test to compare the mean differences against zero, and proportional bias was assessed using linear regression of the differences versus the means of the two measurements. $P<0.05$ was considered statistically significant. No significant fixed or proportional bias was observed across all parameters ($P>0.05$). 3D-CT: Three-dimensional computed tomography; OV: Orbital volume; ICC: Intraclass correlation coefficient; CI: Confidence interval.

Accurate quantification of orbital structures is vital for clinical diagnosis, surgical planning, and post-traumatic reconstruction, especially given that orbital anatomy varies with age, gender, and ethnicity, underscoring the need to account for population-specific differences in precision medicine[5-8]. However, the lack of data on regional orbital anatomical variations within China may limit physicians' ability to make well-informed diagnostic and therapeutic decisions. To address this gap, we conducted a 3D-CT comparative analysis of orbital structures in two geographically distinct Chinese populations. Traditional two-dimensional cephalometric methods are prone to landmark distortion due to cranial positioning errors and limited visibility of structures across slices[20-21]. In contrast, 3D cephalometry corrects positional bias, preserves complete anatomical information, and reduces measurement discrepancies[20,22]. Prior studies have demonstrated its high accuracy and reproducibility[23-25], which is consistent with the excellent repeatability observed in our analysis (Table 5).

Clinically, precise 3D morphometric assessment is crucial for orbital floor and medial wall reconstruction, especially in cases of bilateral orbital trauma where the absence of contralateral references complicates volume correction[26-27]. In this context, our findings highlight that population-specific orbital geometry may influence surgical safety and efficacy. The Southern China cohort exhibited greater orbital height (35.98±1.66 *vs* 34.83±1.88 mm) and OI (95.55±6.59 *vs* 91.91±4.72), consistent with the Megaseme orbital type typical of East Asian craniofacial morphology[17,28]. In contrast, the Kashi cohort presented transitional features characterized by smaller orbital height and index. These anatomical distinctions have direct clinical implications. These observations suggest that, for Kashi patients, implants should prioritize horizontal contour and basal support to restore OV accurately. For Southern China patients, the slightly taller orbits require implants that accommodate the greater vertical dimension, but the main focus remains on matching overall orbital shape and volume. In both populations, careful preoperative 3D assessment ensures implants are tailored to individual orbital geometry, optimizing anatomical and functional outcomes[29-31]. Exophthalmos serves as both a critical diagnostic marker and surgical indicator across orbital pathologies, including orbital fractures, thyroid-related eye diseases, and intra-orbital space-occupying lesions[32-34]. Our study revealed the Southern China individuals exhibited significantly greater exophthalmos (16.60±2.15 *vs* 15.49±1.81 mm; $P=0.014$). Traditionally measured using a Hertel exophthalmometer, exophthalmos assessment is prone to considerable inter-observer variability[32-33]. Recent advances favor CT and magnetic resonance imaging (MRI) as more reliable modalities, as they avoid the confounding effects of facial asymmetry[5,11]. Previous studies have confirmed racial differences in ocular protrusion[15-18,35]. For example, Wu *et al*[36] reported an average ocular protrusion of 15 mm in Han adults from northeastern China using a Hertel exophthalmometer (*n*=2010). Kashkouli *et al*[15] reported an average of 14.7±2.3 mm in Iranian adults (*n*=455). These variations have two key clinical implications. First, individuals from Southern China may possess narrower physiological margins before pathological protrusion is reached, whereas Kashi patients may require greater changes to cross diagnostic thresholds. Second, standardized diagnostic criteria must consider population-specific norms to ensure accuracy. Given the known inter-observer variability in Hertel measurements, clinical protocols should incorporate region-specific imaging references, adopt dynamic thresholds based on population deviations, and emphasize longitudinal monitoring relative to baseline rather than relying solely on absolute values[22].

The Keros classification provides essential guidance for medial orbital wall decompression through stratification of intracranial entry risk based on the depth of the OF and height of the cribriform plate[6,37]. Although our study found no statistically significant difference in the mean OF depth between Southern China and Kashi populations, the proportion of Keros type III cases was notably higher in Southern China (*n*=4) compared to

the Kashi group (n=1). Given that Keros type III corresponds to a deeper OF, this anatomical variant substantially increases the risk of iatrogenic dural injury or cerebrospinal fluid leakage during medial wall decompression[37]. Region-specific preoperative imaging review and tailored surgical protocols, including limiting ethmoidectomy depth or employing image-guided navigation, are particularly warranted in Southern Chinese patients.

In deep lateral decompression, the sphenoid trigone is a triangular region bounded posteriorly by the middle cranial fossa and directly determines the width of the surgical corridor and the safety margin[10,30-31]. Preserving the cortical bone at this boundary helps prevent cerebrospinal fluid leakage[18]. In this study, Kashi subjects exhibited significantly shorter sphenoid trigone lengths (11.25±3.14 *vs* 12.64±3.19 mm; P=0.033) and narrower widths [7.43 (3.02) mm *vs* 8.83 (3.26) mm; P=0.016] compared with their Southern Chinese counterparts. These structural differences suggest a more confined lateral surgical corridor in the Kashi group, potentially limiting decompression extent and increasing the technical challenge. For comparison, Shin *et al*[18] reported considerably larger dimensions in Korean subjects (length: 23.4±2.6 mm; posterior depth: 36.3±2.8 mm; n=60), identifying the area within 3 cm of the lateral orbital rim as the safe zone for decompression. The differences between these studies likely arise from variations in the horizontal plane used to measure the sphenoid trigone as well as population-specific craniofacial characteristics. Nevertheless, the approximately 10%–15% reduction in sphenoid trigone dimensions in the Kashi population indicates that surgeons should anticipate a narrower operative field and reduce posterior bone removal by 1–2 mm compared with conventional East Asian parameters to avoid breaching the middle cranial fossa. Therefore, preoperative 3D-CT assessment of sphenoid trigone morphology is strongly recommended to individualize decompression extent and ensure surgical safety.

While this study provides novel insights into orbital anatomy through systematic 3D-CT comparisons between Kashi and Southern Chinese populations, several limitations should be acknowledged. First, the sample was drawn from only two medical centers, which may not fully capture the broader anatomical diversity within each region. Second, although the sample size was sufficient for an initial comparative analysis, it was relatively modest, precluding further stratified analyses by age and potentially limiting the generalizability of some findings. Additionally, minor measurement bias may exist due to differences in CT scanner models, despite standardized parameters. Therefore, future studies with larger, multi-center cohorts encompassing diverse subpopulations are warranted to validate and extend these preliminary observations.

In summary, this work establishes the first quantitative atlas of region-specific orbital anatomy across China's geographically distinct populations, delineating clinically significant disparities in morphometric parameters. These findings carry meaningful clinical implications for orbital disease assessment, surgical planning and personalized risk stratification. Future studies should prioritize integrating region-specific normative data into imaging evaluation protocols and surgical training curricula, particularly in ethnically diverse regions. Incorporating anatomical diversity into precision medicine frameworks will be essential to improving surgical outcomes and minimizing complications in orbital procedures.

ACKNOWLEDGEMENTS

Authors' Contributions: Wang M and Yang Y, contributed equally to this work and share co-first authorship. They were primarily responsible for the study design, data collection, analysis, and manuscript writing. Cao SJ, Tang JJ, Li JM, Bao YK, Zhang ZH, Gao Y, Liu YM, Kuerban M, Abulizi T, Su SC, and Huang WF were involved in conducting the experiments, organizing the data, and providing critical revisions to the manuscript. Jiang AX and Lu R are the corresponding authors. They conceived and supervised the study, and they provided important revisions to the manuscript and approved the final version.

Foundations: Supported by Research Funds of the State Key Laboratory of Ophthalmology (No.2025QZSPT05); Young Doctoral Startup Project of Guangzhou Basic and Applied Basic Research Project (No.2024A04J4475); Guangdong Basic Research Center of Excellence for Major Blinding Eye Diseases Prevention and Treatment (No.2024-PIZC-039; No.2024-YXGG-008).

Conflicts of Interest: Wang M, None; **Yang Y,** None; **Cao SJ,** None; **Tang JJ,** None; **Li JM,** None; **Bao YK,** None; **Zhang ZH,** None; **Gao Y,** None; **Liu YM,** None; **Kuerban M,** None; **Abulizi T,** None; **Su SC,** None; **Huang WF,** None; **Jiang AX,** None; **Lu R,** None.

REFERENCES

1 Salgado-López L, Campos-Leonel LCP, Pinheiro-Neto CD, *et al*. Orbital anatomy: anatomical relationships of surrounding structures. *J Neurol Surg B Skull Base* 2020;81(4):333-347.

2 Agosti E, Alexander AY, Plou P, *et al*. 360° around the orbit: key surgical anatomy of the microsurgical and endoscopic cranio-orbital and orbitocranial approaches. *Neurosurg Focus* 2024;56(4):E2.

3 Santos LAR, Javate RM. An anatomical study of the medial wall, lateral wall, roof, and floor of the Filipino orbit. *Adv Ophthalmol Pract Res* 2025;5(1):73-77.

4 Serioli S, Nizzola M, Plou P, *et al*. Surgical anatomy of the microscopic and endoscopic transorbital approach to the middle fossa and cavernous sinus: anatomo-radiological study with clinical applications. *Cancers (Basel)* 2023;15(18):4435.

5 Hierl KV, Krause M, Kruber D, *et al*. 3-D cephalometry of the the orbit regarding endocrine orbitopathy, exophthalmos, and sex. *PLoS One* 2022;17(3):e0265324.

6 Chan MA, Ibrahim F, Kumaran A, *et al*. Ethnic variation in medial orbital wall anatomy and its implications for decompression surgery. *BMC Ophthalmol* 2021;21(1):290.

7 Scendoni R, Kelmendi J, Arrais Ribeiro IL, *et al*. Anthropometric analysis of orbital and nasal parameters for sexual dimorphism: New anatomical evidences in the field of personal identification through a retrospective observational study. *PLoS One* 2023;18(5):e0284219.

8 Wu M, Salinero LK, Chang AE, *et al*. Quantitative analysis of male versus female frontal bone and orbital skeletal morphology. *Plast Reconstr Surg Glob Open* 2025;13(9):e7068.

9 Cheng SN, Ming YC, Hu M, *et al*. Risk prediction of dysthyroid optic neuropathy based on CT imaging features combined the bony orbit with the soft tissue structures. *Front Med (Lausanne)* 2022;9:936819.

10 Kitaguchi Y, Takahashi Y, Kakizaki H. Computed tomography–based prediction of exophthalmos reduction after deep lateral orbital wall decompression for Graves' orbitopathy. *Graefes Arch Clin Exp Ophthalmol* 2019;257(12):2759-2767.

11 Bao YK, Zhang ZH, Li C, *et al*. Geometric and volumetric measurements of orbital structures in CT scans in thyroid eye disease classification. *Appl Sci* 2021;11(11):4873.

12 He B, Kim Y, Ngo Q. Orbital remodeling and 3-dimensional printing in delayed orbital floor fracture reconstructions. *Plast Reconstr Surg Glob Open* 2025;13(5):e6772.

13 Hahn HM, Jung YK, Lee IJ, *et al*. Revisiting bilateral bony orbital volumes comparison using 3D reconstruction in Korean adults: a reference study for orbital wall reconstruction, 3D printing, and navigation by mirroring. *BMC Surg* 2023;23(1):351.

14 Office of the Leading Group of the State Council for the Seventh National Population Census. Main Data of the Seventh National Population Census. *Beijing: China Statistics Press* 2021:127.

15 Kashkouli MB, Nojomi M, Parvaresh MM, *et al*. Normal values of hertel exophthalmometry in children, teenagers, and adults from Tehran, Iran. *Optom Vis Sci* 2008;85(10):1012-1017.

16 Bilen H, Gullulu G, Akcay G. Exophthalmometric values in a normal Turkish population living in the northeastern part of Turkey. *Thyroid* 2007;17(6):525-528.

17 Patra A, Singla RK, Mathur M, *et al*. Morphological and morphometric analysis of the orbital aperture and their correlation with age and gender: a retrospective digital radiographic study. *Cureus* 2021;13(9):e17739.

18 Shin KJ, Lee SH, Ha TJ, *et al*. Position and size of the sphenoid door jamb in the lateral orbital wall for the orbital decompression. *Anat Cell Biol* 2019;52(3):242.

19 Ramakrishnan VR, Suh JD, Kennedy DW. Ethmoid skull-base height: a clinically relevant method of evaluation. *Int Forum Allergy Rhinol* 2011;1(5):396-400.

20 Chen SN, Chen L, Diao JL, *et al*. Research progress in clinical application of three-dimensional reconstruction in orbital measurement. *Zhonghua Yan Ke Za Zhi* 2023;59(1):58-62.

21 Ji YR, Qian ZQ, Dong Y, *et al*. Quantitative morphometry of the orbit in Chinese adults based on a three-dimensional reconstruction method. *J Anat* 2010;217(5):501-506.

22 Otu E, Nalçacı Bozkurt N, Örmeci T, *et al*. 3D evaluation of bony orbit characteristics in relation to age, sex, and symmetry: a quantitative CT study. *Acta Radiol* 2025:02841851251326162.

23 Smektała T, Jędrzejewski M, Szyndel J, *et al*. Experimental and clinical assessment of three-dimensional cephalometry: a systematic review. *J Cranio Maxillofac Surg* 2014;42(8):1795-1801.

24 Regensburg NI, Kok PHB, Zonneveld FW, *et al*. A new and validated CT-based method for the calculation of orbital soft tissue volumes. *Invest Ophthalmol Vis Sci* 2008;49(5):1758.

25 Erdem H, Tekeli M, Cevik Y, *et al*. Three-dimensional (3D) analysis of orbital morphometry in healthy Anatolian adults: sex, side discrepancies, and clinical relevance. *Cureus* 2023;15(9):e45208.

26 Mansour TN, Rudolph M, Brown D, *et al*. Orbital blowout fractures: a novel CT measurement that can predict the likelihood of surgical management. *Am J Emerg Med* 2017;35(1):112-116.

27 Yao BC, He Y, Jie BM, *et al*. Reconstruction of bilateral post-traumatic midfacial defects assisted by three-dimensional craniomaxillofacial data in normal Chinese people—a preliminary study. *J Oral Maxillofac Surg* 2019;77(11):2302.e1-2302.e13.

28 Botwe BO, Sule DS, Ismael AM. Radiologic evaluation of orbital index among Ghanaians using CT scan. *J Physiol Anthropol* 2017;36(1):29.

29 Chang JT, Morrison CS, Styczynski JR, *et al*. Pediatric orbital depth and growth: a radiographic analysis. *J Craniofacial Surg* 2015;26(6):1988-1991.

30 Scarabosio A, Surico PL, Singh RB, *et al*. Thyroid eye disease: advancements in orbital and ocular pathology management. *J Pers Med* 2024;14(7):776.

31 Ong AA, DeVictor S, Vincent AG, *et al*. Bony orbital surgery for Graves' ophthalmopathy. *Facial Plast Surg* 2021;37(6):692-697.

32 Golan S, Rootman DB, Lambros V, *et al*. Ocular protrusion in sitting and supine position. *Clin Exp Ophthalmol* 2018;46(7):836-837.

33 Bingham CM, Sivak-Callcott JA, Gurka MJ, *et al*. Axial globe position measurement: a prospective multicenter study by the international thyroid eye disease society. *Ophthalmic Plast Reconstr Surg* 2016;32(2):106-112.

34 Sheth NT, Lee IT, Stinnett SS, *et al*. Relative exophthalmos in facial nerve palsy. *Can J Ophthalmol* 2025;60(5):e667-e671.

35 Migliori ME, Gladstone GJ. Determination of the normal range of exophthalmometric values for black and white adults. *Am J Ophthalmol* 1984;98(4):438-442.

36 Wu D, Liu X, Wu D, *et al*. Normal values of hertel exophthalmometry in a Chinese Han population from Shenyang, Northeast China. *Sci Rep* 2015;5:8526.

37 Gauba V, Saleh GM, Dua G, *et al*. Radiological classification of anterior skull base anatomy prior to performing medial orbital wall decompression. *Orbit* 2006;25(2):93-96.